EFFECT OF BUTANOL BLEND ON IN-CYLINDER COMBUSTION PROCESS. PART 1: SPARK IGNITION ENGINE

Cinzia Tornatore, Luca Marchitto, Alfredo Mazzei, Gerardo Valentino, Felice E. Corcione, Simona S. Merola

Istituto Motori – CNR
G. Marconi Street 8 – 80125 Napoli, Italy
e-mail: s.merola@im.cnr.it

Abstract

The addition of alcohol to conventional hydrocarbon fuels for a spark-ignition engine can increase the fuel octane rating and the power for a given engine displacement and compression ratio. In this work, the influence of butanol addition to gasoline in a port fuel-injection, spark ignition engine was investigated. The experiments were realized in a single cylinder ported fuel injection SI engine with an external boosting device. The optical accessible engine was equipped with the head of commercial SI turbocharged engine with the same geometrical specifications (bore, stroke, compression ratio) as the research engine. The effect on the spark ignition combustion process of 40% n-butanol blended in volume with gasoline was investigated by cycle resolved visualization. The engine worked at low speed, medium boosting and wide open throttle. Changes in spark timing and fuel injection phasing were considered in order to investigate normal and abnormal combustion. Comparisons between the parameters related to the flame luminosity and to the pressure signals were performed. The duration of injection for butanol blend was increased to obtain stoichiometric mixture. In open valve injection condition, the fuel deposits on intake manifold and piston surfaces decreased, allowing a reduction in fuel consumption. Butanol blend granted the performance levels of gasoline and in open valve injection allowed to minimize the abnormal combustion effects and the formation of ultrafine carbonaceous particles.

Keywords*: Optical diagnostics; Combustion process; PFI SI boosted engine; Butanol–gasoline blend*

1. Introduction

Butanol can be used in the internal combustion engine designed for working with gasoline without modification. Butanol can be produced from biomass (biobutanol) as well as fossil fuels (petrobutanol). Both the fuels have the same chemical properties. Recent studies on biobutanol have shown that it has the potential to play a significant role in a sustainable, non-petroleum-based, industrial system [1, 2]. In regard to overall biomass utilization, butanol has a key advantage over ethanol, the most established biofuel, as butanol can be produced from both five and six carbon sugars without organism modification. In addition to cellulose, this allows for the efficient use of hemicellulose, which accounts for 20–40% of biomass. [3, 4]

Butanol has a number of advantages over other common alcohol fuels such as ethanol and methanol. [4] The net heat of combustion of butanol is roughly 83% that of gasoline compared with 65 and 48% for ethanol and methanol, respectively [5]. Butanol is far less hygroscopic than methanol, ethanol and propanol. These lower alcohols are fully miscible with water, whereas butanol has only modest water solubility. This allows low energy intermediate purification step. [6] Butanol is less corrosive than ethanol, can be transported in existing pipelines and is much safer to work with than lower alcohols based on its relatively high boiling point and flashpoint. [4] As for ethanol, the adding of butanol to conventional hydrocarbon fuels for use in a spark-ignition engine can increase fuel octane rating and power for a given engine displacement and compression ratio, thereby reducing fossil-fuel consumption and CO_2 emissions [7-9]. Ethanol use for spark-ignition engines has been widely investigated. While, the almost totality of studies about butanol–

gasoline blends consisted in the evaluation of performance, fuel consumption and exhaust emissions for different engine operating conditions [10-13]. These research activities demonstrated that the concentrations of 20-40% butanol in gasoline enabled to run the engine at leaner mixture than gasoline for fixed performance. These blends offered similar UHC emissions than gasoline, which increased at higher butanol concentrations. The blends decreased the NOx emissions to a lower level than with pure gasoline at its leanest mixture. The slight increase in SFC was related to the blend's reduced combustion enthalpy. [10, 14] On the other hand, recent works on the performance of an engine fuelled with different mixing fractions of gasoline-butanol blends demonstrated a reduction in brake specific energy consumption and reduction emissions. [15]

This paper investigates the in-cylinder phenomena correlated with butanol–gasoline combustion in spark ignition (SI) engine. To this goal, cycle resolved visualization was performed to follow the flame propagation from the spark ignition to the late combustion phase. The experiments were realized in a single cylinder ported fuel injection (PFI) SI boosted engine. Butanol/gasoline blend was tested for several engine operating conditions. Changes in spark timing and fuel injection phasing were considered. Comparisons between the parameters related to flame luminosity and to pressure signals were performed.

2. Experimental apparatus

The experiments were performed in an optically accessible single cylinder PFI SI engine. It was equipped with the cylinder head of a SI turbocharged engine with the same geometrical specifications (bore, stroke, compression ratio) as the research engine. Further details on the engine are reported in Tab. 1. The head had four valves and a centrally located spark plug. The injection system was the same as the reference real engine with a commercial 10 holes injector. An external device allowed the control of the intake air pressure, in a range of 1000 - 2000 mbar, and of the temperature, in a range of 290 – 340 K. A quartz pressure transducer was flush-installed in the region between intake-exhaust valves at the side of the spark plug.

Tab. 1. Specifications of the single cylinder PFI boosted engine

Displaced volume	399 cc
Stroke	81.3 mm
Bore	79 mm
Connecting Rod	143 mm
Compression ratio	10:1

The transducer allowed to perform in-cylinder pressure measurements in real-time. An elongated engine piston was used, it was flat and its upper part was transparent since it was made of fused silica UV enhanced (Φ=57mm). To reduce the window contamination by lubricating oil, self-lubricant Teflon-Bronze composite piston rings were used in the optical section. To reduce the initial conditions effects, the engine was preheated by a conditioning unit, and it was maintained in motored condition by an electrical engine until the water temperature reached 65ºC.

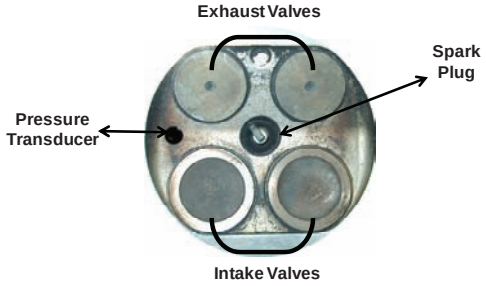

Fig. 1. Bottom field of view of the combustion chamber

After the warm-up, the engine worked in fired conditions for 300 consecutive cycles. The engine parameters and pressure measured in the last 200 cycles were considered in the work. Then the engine returned in motored condition for 100 cycles. This phase allowed checking a possible change in thermal and fluid-dynamic status of the engine from the beginning of the measurements. During the combustion process, the light passed through a quartz window located in the piston and it was reflected toward the optical detection assembly by a 45° inclined UV-visible mirror placed at the bottom of the engine. Cycle resolved flame visualization was performed using an Optronis "CamRecord 5000" high speed camera. It was a CMOS monochrome image sensor, its full chip dimension was 512x512 pixel and the pixel size was 16x16 μm. The camera A/D Conversion was 8 bit and the spectral range extended from 390 nm to 900 nm. The camera was equipped with a 50 mm focal Nikon lens, a camera region of interest was selected (480 x 480 pixel) to obtain the best match between spatial and temporal resolution. All the images are a line-of-sight average. The optical assessment allowed a spatial resolution in 2D field of view around 0.12 mm/pixel. The exposure time was fixed at 10 μs and the frame rate was 5392 fps. In this work the optical measurements were performed during 100 consecutive engine cycles after an engine warm-up under motored conditions and 100 fired cycles. Fig. 1 shows the bottom field of view of the combustion chamber. National Instruments LabVIEW acquisition-system driven by an optical encoder with 0.2 crank angle degree resolution recorded the TTL signals from the high-speed camera acquisitions and the pressure transducer. In this way, it was possible to determine the crank angles at which the optical measurements were carried out.

Tab. 2. Fuel specifications

	Gasoline	Butanol
Low heating value (MJ/kg)	43.5	32.0
Latent heat of vaporization (kJ/L)	223	474
RVP (kPa)	60-90	18.6
A/F stoichiometric	14.6	11.1
Density (kg/m3)	720-775	813
Oxygen (% weight)	< 2.7	21.6
RON	95	113
Adiabatic flame temperature (K)	2370	2340

Tab. 3. Fuel injection conditions

label	fuel	SOI	DOI
GAS_OV	gasoline	300°BTDC	133 CAD
GAS_CV	gasoline	130°ATDC	148 CAD
BU40_OV	BU40	300°BTDC	153 CAD
BU40_CV	BU40	130°ATDC	165 CAD

In-house LabVIEW numerical procedure was applied for the retrieving of the experimental data. Regarding the optical data, the 8-bit grey-scale image was converted in a numerical matrix. In this way it was possible to evaluate the luminous signals locally or as integral on the whole combustion chamber. To quantify the variability of indicated work per cycle, the Coefficient Of Variation of Indicated Mean Effective Pressure (COV_{IMEP}) was calculated as COV [%] = 100*σ/μ where σ is the standard deviation and μ is the mean IMEP taken over 200 cycles. The IMEP was

calculated by the integration of (P·dV) over a cycle divided by the displacement volume of the cylinder. [16] Combustion tests were carried out using two fuels. The baseline fuel was the commercial gasoline. The comparison fuel was obtained by blending in volume 60% of the baseline gasoline and 40% of n-butanol with a purity of 99.99% (Tab. 2). The blend was indicated in the following as BU40.

3. Results and Discussion

All the tests presented in this paper were carried out at an engine speed of 2000 rpm and wide open throttle. Absolute intake air pressure and temperature were fixed at 1.4 bar and 338 K, respectively. The relative injection pressure was settled at 3.5 bar. The injection timings were fixed at 130 CAD ATDC and 300 CAD BTDC in order to inject the fuel at closed intake valves (CV) and open intake valves (OV), respectively. The spark timing was changed in order to identify the maximum brake torque and the knocking limit. To distinguish normal combustion cycles from knocking cycles, the knocking signal was evaluated through 5 - 30 kHz band-pass filtering of the pressure signals [16], [17]. The knocking limit was reached when more than 40% of the engine cycles in a test case showed a knocking pressure > 5% of the motored pressure. [18-20] The duration of injection (DOI) was changed in order to set $\lambda = 1.0$ (±1%) as measured by a lambda sensor at the engine exhaust and averaged over 200 consecutive engine cycles. The fuel injection conditions are resumed in Tab. 3. The first evidence is the difference in the open valve and close valve injection. In a port-fuel-injected engine, the fuel is generally injected at the backside of a closed intake valve to take advantage of the warm valve and port surfaces for vaporization. [21-24]

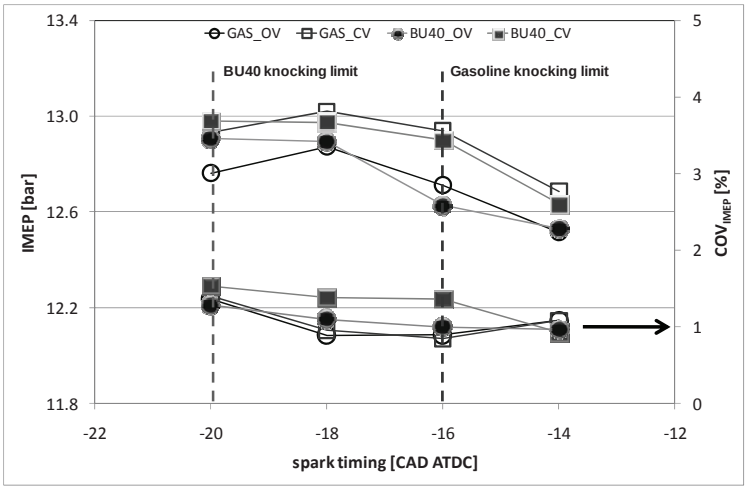

Fig. 2. IMEP value and COV_{IMEP} versus spark timing evaluated for the selected conditions

However, a large part of the injected spray is deposited on the intake manifold surfaces and forms a layer of liquid film on the valve and port surfaces. The film needs to be re-atomized by the shearing airflow as the intake valves open. If these fuel layers are not well atomized they enter the cylinder as drops and ligaments [24]. These phenomena occur in varying degrees and depend upon the engine design, injector location and engine operation. Previous experiments on the same engine fuelled by gasoline demonstrated that the injector sprayed the fuel towards the plate between the intake valves and on the intake valves stems [25], [26]. The droplets impingement induced fuel layer formation on the intake manifold walls. The fuel layers were drawn by gravity on the valve head and gap, where they remained as film due to the surface tension. The stripping of the squeezed fuel film created fuel deposits on the optical window. [18][21] When the injection occurred in open valve condition, part of the droplets was carried directly into the combustion chamber by the gas flow. These droplets sucked in the combustion chamber stuck on the cylinder

walls. In both injection conditions, the fuel deposits on the combustion chamber walls created fuel-rich zones on the piston surfaces that influenced the composition of the mixture charge and hence the combustion process. During the normal combustion process only part of the fuel deposits were completely burned. Thus more fuel should be injected to reach the selected air-fuel ratio measuring at the exhaust [20]. In the open valve injection the fuel deposits amount and size were smaller than closed valve injection, thus the duration of injection resulted shorter [24][26]. Regarding the difference in the injection duration between gasoline and BU40, as with any alcohol, gasoline-butanol blends have a lower stoichiometric air-fuel ratio. Therefore, when using gasoline blended with butanol, fuel flow must be increased to ensure the same relative air-fuel ratio as with pure gasoline.

Figure 2 gives the curves of IMEP and COV_{IMEP} versus spark timing for the selected operating conditions. These values were obtained as average on 200 consecutive engine cycles. At fixed spark timing, the IMEP range resulted lower than 5% for all conditions and fuels. The IMEP for gasoline fuel increased with the spark advancing and it reached the highest value at 20°BTDC. Similar trend was measured for BU40, which on the other hand maintained same IMEP value at more advanced spark timing. For both fuels the IMEP for CV injection was higher than OV, in agreement with the results reported in previous works. [25][26] For each injection fuel, the IMEP for BU40 was very close to gasoline; this agrees with the results reported in [27] in which at full load, the power drop is significant only for butanol concentrations higher than 30-40 %.

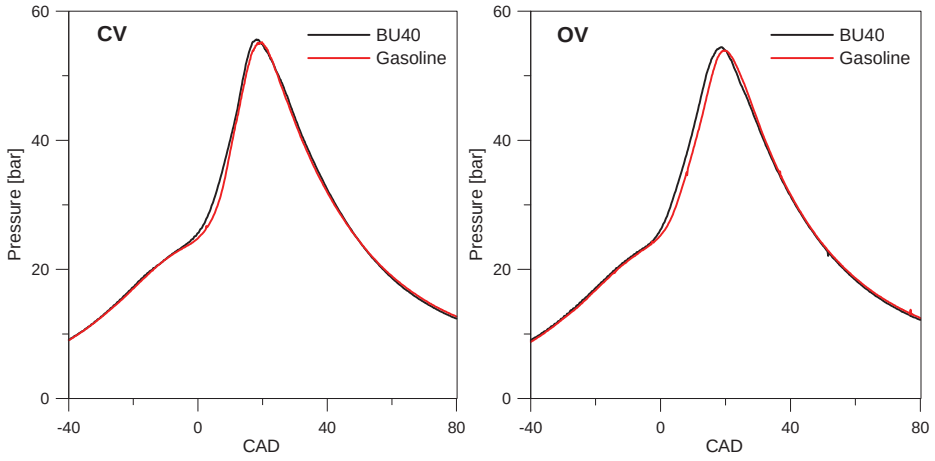

Fig. 3. In-cylinder pressure signals measured for closed valve (CV) and open valve (OV) injection conditions

About the spark timing effect, for gasoline fuel, the knocking limit was evaluated around 16°BTDC for both fuel injection conditions. For BU40, the knocking limit advanced until around 20°BTDC. Thus butanol blend allowed working in more advanced spark timing without negative effects due to the abnormal combustion. The COV_{IMEP} increased with spark advance until reaching the highest value in knocking regime. When the ignition is too delayed, COV_{IMEP} increased with retarding spark timing. It occurs because the cylinder temperature is comparatively low. Besides, the quite low and uneven mixture concentration near the spark plug brings negative influence on the initiation and development of flame kernel. Thus the low combustion efficiency does harm to combustion stability. In this work particular attention was paid to the optical results obtained at 14°BTDC spark timing, in order to evaluate the effect of selected fuels on the normal combustion process at comparable IMEP with satisfactory engine stability. Fig. 3 shows in-cylinder pressure signals of selected engine cycles related to the operating conditions of Tab. 3. The cycles were characterized by the same IMEP (12.65±0.5%) at the fixed spark timing of 14°BTDC. It should be noted that for both injection conditions, pressure peaks were a little bit higher for BU40 and the peak crank angle occurred earlier if compared to gasoline. This result was due to faster n-butanol combustion than gasoline [10][11]. The in-cylinder pressure measurements give real-time cycle-

resolved information on the combustion process, but they furnish overall data and they don't allow local analysis. Cycle resolved visualization is a powerful tool for detailing thermal and fluid dynamic phenomena that occur in the combustion chamber. Fig. 4 and 5 report image selections of the cycle resolved flame front evolution for the gasoline and BU40 in CV and OV conditions, respectively. The images were acquired during the engine cycles of Fig. 3.

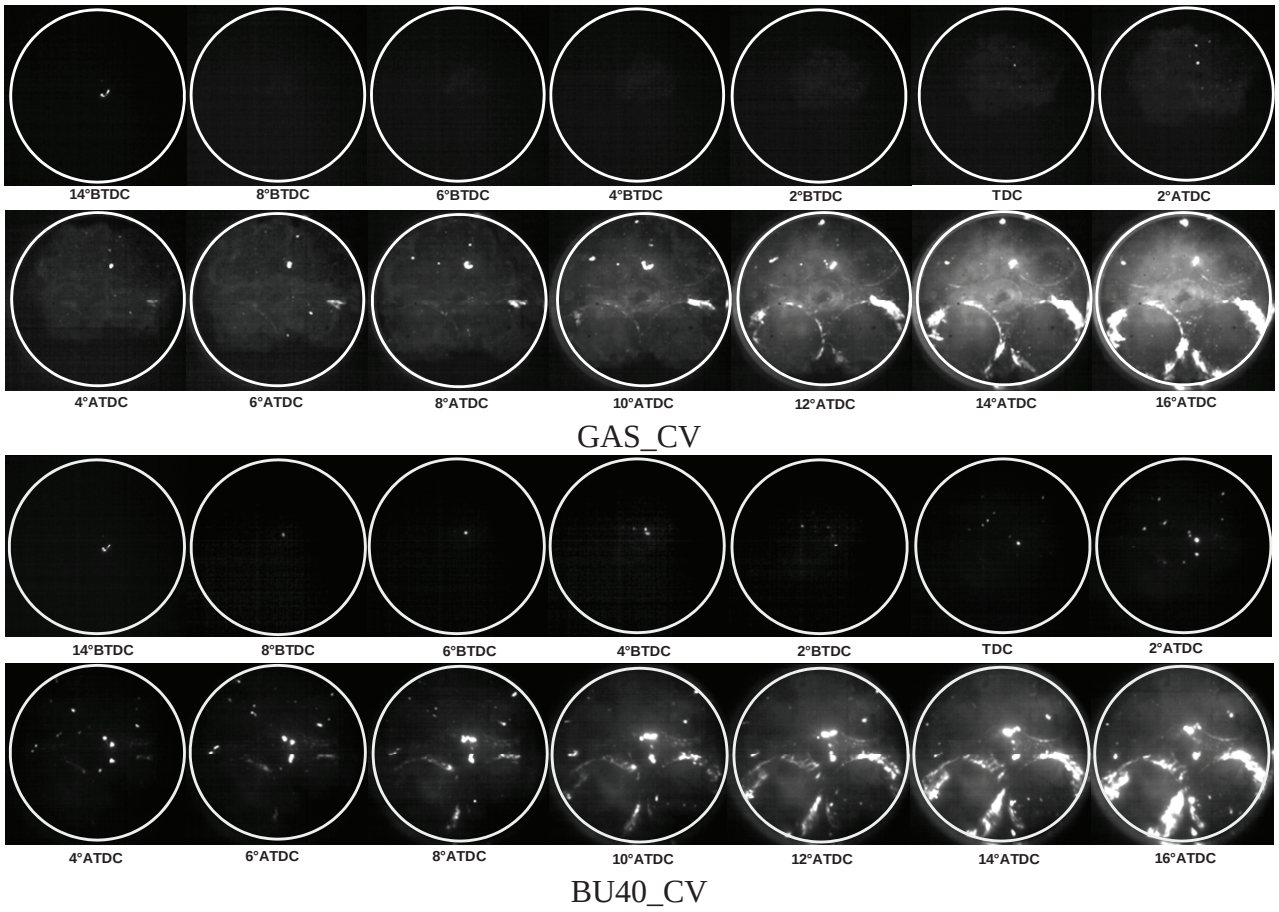

Fig. 4. Selected images of the cycle resolved flame front evolution for the gasoline and BU40 in CV condition. The related combustion pressure signals are reported in Fig. 3

The brightness and contrast of the images were changed in order to enhance the kernel flame luminosity. The images show the combustion process from the spark ignition until the flame front reaches the cylinder walls. In good agreement with [25][26] the flame front started from the centrally located spark plug; the plasma luminosity near the spark plug is detectable in the first frame. Then the kernel spread with radial-like behaviour for around 10 CAD. After this time the flame front shape showed an asymmetry that induced the flame to reach first the cylinder walls in the exhaust valves region around 4°ATDC. This was due to the fuel film deposited on the intake valves and combustion chamber surfaces previously discussed. The fuel film develops dynamically under the effect of the gas flow influencing mixture composition and combustion process. In fact, the flame propagation is influenced by the thermodynamic conditions, mixture composition and local turbulence intensity. When a flame propagates in the normal direction to a region with equivalence ratio gradient, each part of the front evolves in a field with varying fuel concentration. This induces variation of the propagation speed along the flame front and an increase in flame wrinkling, in comparison with the homogeneous case. It should be noted that the asymmetry was less evident for BU40, which showed a more regular evolution of the flame front with slight border wrinkling. This was a first marker of a lower amount of fuel deposits near the valves for the blend than pure gasoline.

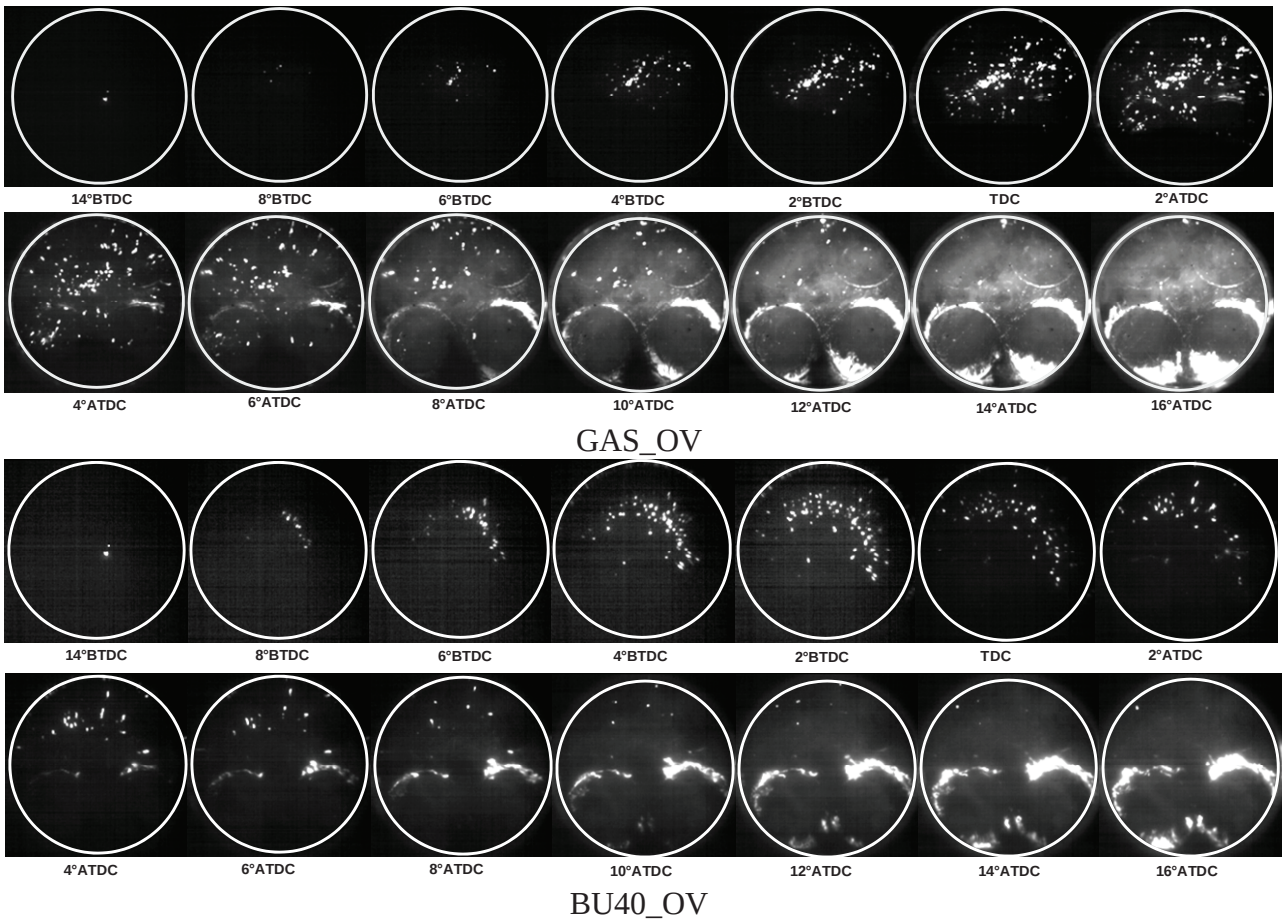

Fig. 5. Selected images of the cycle resolved flame front evolution for the gasoline and BU40 in OV condition. The related combustion pressure signals are reported in Fig. 3

Bright spots were observed in the burnt gas before the flame front reached the chamber walls. The bright spots were due to the fuel deposits on the optical window. During the fuel injection at closed intake valve, when the gas flow passes through the valves, the fuel droplets on the quartz window are stripped from the fuel film layer. After reaching the combustion chamber, the fuel droplets stuck on the piston surfaces. These fuel deposits also created fuel-rich zones that ignited when reached by the normal flame front. In CV condition the spots are bigger but less in number than in OV condition. When the injection occurred in the open valves condition the fuel droplets sticking was enhanced by the partial carrying of the injected fuel droplets directly into the combustion chamber due to the gas flow. The bright spots have a random nature; during the combustion process they decreased in size and number and then they disappeared before the exhaust valve opening [25]. For BU40 the bright spots were less evident than gasoline; the chemical composition of the blend helped the vaporization of the low-volatile component and then the fuel deposits burning. The presence of the fuel deposits as squeezed film or impinged droplets had direct effect on the flame radius evolution in terms of kernel cyclic variability and flame stability. [28] When the flame approached the intake valve region, the heat exchange between the intake ports and the surrounding gas led to the fuel film deposits evaporation. It influenced the composition of the mixture creating locally fuel-rich zones. The higher fuel amount near the intake valves for gasoline in CV condition induced fuel-richer zones that slowed down the flame front more than in the other conditions. When that normal flame front reached the intake valves, the fuel film layer around the valves burned and strong intensity flames were observed [24][29]. The outlines of the valves are clearly distinguished since 8 CAD ATDC for all the tested conditions (Fig. 4-5). Previous works demonstrated that the flame near the valves had diffusion-controlled

nature. Their inception was possible since the oxygen was not completely consumed after the normal flame front propagation [25][26]. The diffusion-controlled flames persisted in the late combustion phase and their optical evidence could be detected until the exhaust valves opening (153 CAD ATDC).

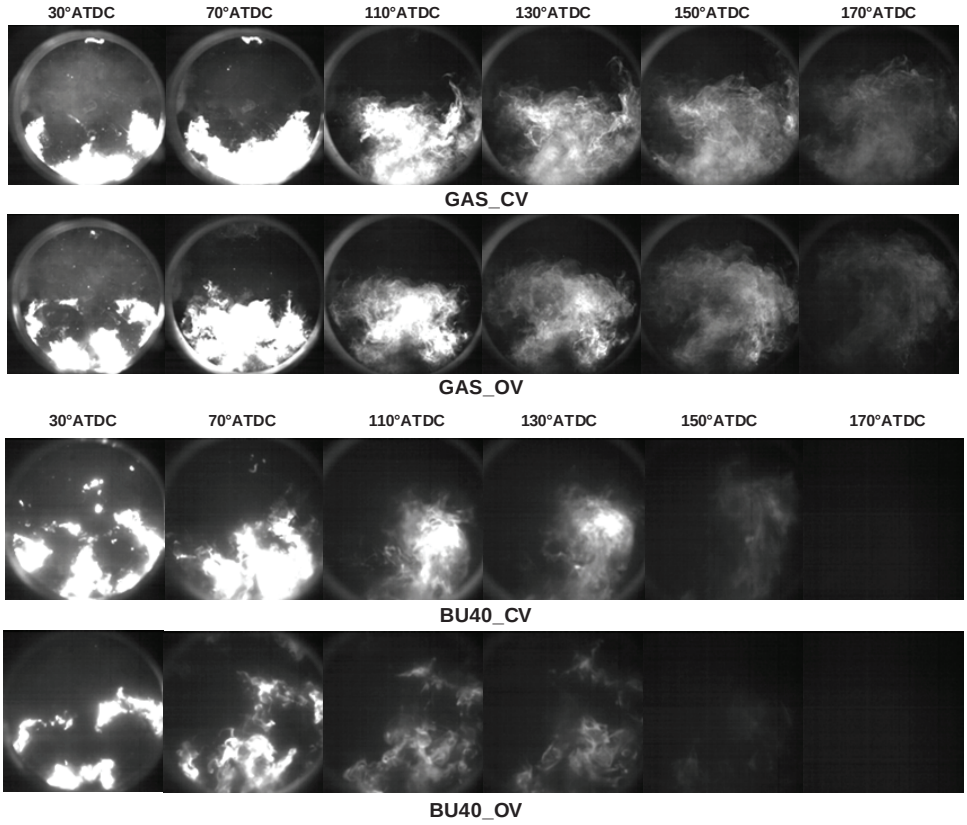

Fig. 6. Cycle resolved visualization of the late combustion phase for the engine cycles of Fig. 3

The spatial distribution of diffusion-controlled flames can be analyzed through the images reported in Fig. 6. For both fuels, in closed valve (CV) injection condition, the flames resulted more intense and with bigger surface than open-valve (OV) due to the higher amount of fuel deposited on the valve stem for CV. Until 70 CAD ATDC, the highest intensity of flames was observed near the intake valves, as expected, for all conditions. Then, different evolutions and spatial distributions were detected.

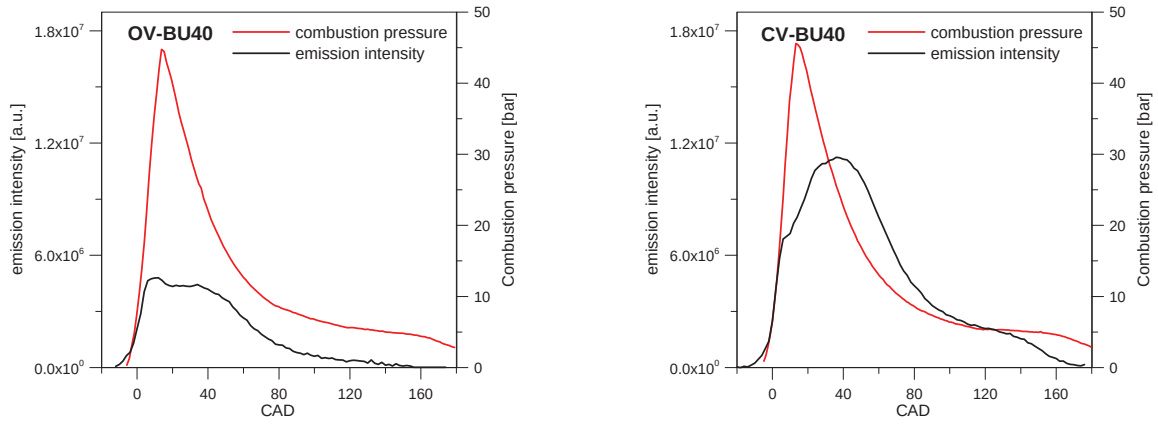

Fig. 8. Comparison between the combustion pressure signal and the integral luminosity measured BU40 with spark timing 20 CAD BTDC

For BU40 the flames spread quickly through the chamber and, around 130 CAD ATDC, their intensities were strongly reduced. This effect was caused by the burning of fuel deposits moved by the gas motion from the intake to the exhaust valves.

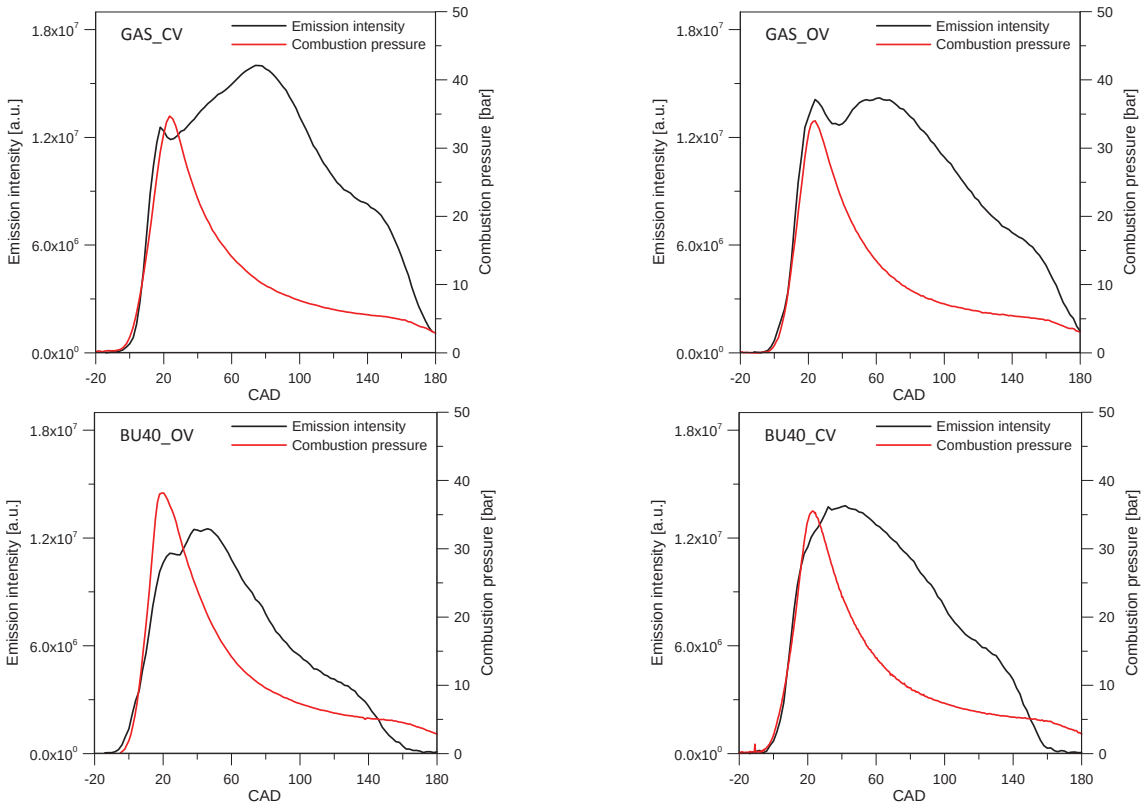

Fig. 7. Comparison between the combustion pressure signal and the integral luminosity measured during the engine cycles plotted in Fig. 3

The diffusion-controlled flames did not contribute to the engine work, and they did not influence the pressure signal [29] In fact, they are surface diffusion flames that warmed up the nearby in-cylinder gas by thermal diffusion. This phenomenon increased the pressure much slower than the reduction of pressure produced by the movement of the piston during the expansion stroke. A comparison between the pressure related measurements and processed optical data was performed. Fig. 7 shows the evolution of the combustion pressure signal and the integral luminosity measured during the engine cycles of Fig. 3. The combustion pressure signal was calculated by the subtraction of the motored in-cylinder pressure from the fired one. From the spark ignition to the maximum values, the luminous and pressure signals showed the same trend for both fuels and injection conditions. In this time the increase in the signals was due to the chemical reactions occurring in the first times of the combustion process that are exothermic and radiative and are characterized by OH, HCO and CH. The behaviours of the combustion pressures and luminous intensities were quite different after the maximum of the signals. Around 30-50 CAD ATDC, the luminous signal showed a smooth increasing while the pressure signal rapidly decreased. These trends were due to the fuel deposits that ignited when the normal flame front reached them. Thus even if the diffusion-controlled flames were strongly intense, their contribution to the combustion pressure was negligible. This occurred also for the gasoline fuel in CV condition that showed the highest diffusion controlled flame luminosity.

Previous spectroscopic investigations and two-colour pyrometry measurements for gasoline fuel showed that the diffusion-controlled flames are characterized by the typical optical markers of carbonaceous structures. [25] The spectra were characterized by a strong continuous contribution that increased with the wavelength in the visible range. This was typical of blackbody-like

emission of the soot precursors. The different levels of intensity were related to different soot concentrations. Thus the open-valve condition showed not only a different spatial distribution of diffusion-controlled flame if compared to the closed-valve condition but also a different time evolution of soot and particulate matter. The results confirmed those in [30] that assigned to the fuel deposition burning the cause of the volatile organic carbon compounds and soot particle emission at the SI PFI exhaust. Thus according to the signals of Fig. 7, for gasoline, until 80 CAD ATDC, the soot formation mechanism was favoured and the soot concentration increased. Then a decrease in soot concentration occurred due to the soot oxidation. Anyway, the soot reduction rate at the exhaust valves opening was not sufficient to oxidize all the particulate; the visible luminosity decrease was due to the gas motion to the exhaust.

For BU40, the mechanism of soot formation and oxidation occurred simultaneously since 40 CAD ATDC, inducing a smooth decrease within 140 CAD ATDC. At this time a sharp soot reduction was observed. The same trend was observed for gasoline around 160 CAD ATDC principally due to the opening of the exhaust valves. It should be noted that BU40 with spark timing until 20 CAD BTDC showed high IMEP with a good combustion stability (COV≅1) without knocking troubles for the same fuel injection duration of previous conditions, as reported in Fig. 2. Moreover, as shown in Fig. 8, the soot integral luminosity confirmed the advantage of the open valve injection than the closed valve injection. Finally the soot luminosity was very lower in intensity if compared to the data measured at spark timing 14 CAD BTDC.

These relevant results demonstrated that medium-low percentage of butanol in the gasoline allowed the reduction in the emission of ultrafine carbonaceous particles. Even if an increase in the fuel injected amount should be considered to obtain the same air-fuel ratio for butanol-gasoline blend if compared to pure gasoline, the better efficiency of fuel deposits burning allowed reducing that amount.

4. Conclusions

The effect on the spark ignition combustion process of 40% n-butanol blended in volume with 60% gasoline (BU40) was investigated through cycle resolved visualization applied in a single cylinder PFI SI engine working at low speed, medium boosting and wide open throttle. BU40 allowed working in more advanced spark timing without negative effects of abnormal combustion. To work with a stoichiometric mixture for both fuels, the duration of injection (DOI) was slightly increased for blend. DOI in closed valve injection (CV) resulted longer than in open valve (OV) for both fuels because in CV injection part of the injected spray is deposited on the intake manifold surfaces forming a layer of liquid film. If these fuel layers are not well atomized they enter the cylinder as drops and ligaments. During the normal combustion process only part of the fuel deposits were completely burnt. Thus more fuel should be injected to reach the selected air-fuel ratio measured at the exhaust. When the normal flame front reached the fuel deposits, strongly intense diffusion-controlled flames were detected. Their contribution to the combustion pressure was negligible. The different levels of intensity were related to different carbonaceous structures and soot precursors concentrations. CV condition was characterized by higher fuel deposition amount and thus more intense diffusion controlled flames than OV. Gasoline in CV condition showed the highest luminosity and BU40 in OV condition the lowest one. This demonstrated that BU40_OV allowed the reduction in emission of ultrafine carbonaceous particles and the optimization of fuel consumption at fixed performance.

References

[1] Harvey, B. G., Meylemans, H. A., *The role of butanol in the development of sustainable fuel technologies*, J. Chem. Technol. Biotechnol, Vol. 86, pp. 2–9, 2011.

[2] Ezeji, T. C., Qureshi, N., Blaschek, H. P., *Bioproduction of butanol from biomass: from genes to bioreactors*, Current Opinion in Biotechnology, Vol. 18, 3, pp. 220–227, 2007.

[3] Angenent, L. T., *Energy biotechnology: beyond the general lignocellulose-to-ethanol pathway,* Current Opinion in Biotechnology, Vol. 18, pp.191–192, 2007.
[4] Yang, H., Yan, R., Chen, H., Zheng, C., Lee, D. H., Liang, D. T., *In-depth investigation of biomass pyrolysis based on three major components: hemicellulose, cellulose and lignin,* Energy Fuels, Vol. 20, pp. 388–393, 2006.
[5] Veloo, P. S., Wang, Y. L., Egolfopoulos, F. N., Westbrook, C. K., *A comparative experimental and computational study of methanol, ethanol, and n-butanol flames,* Combustion and Flame, Vol. 157, 10, pp. 1989-2004, 2010.
[6] Ramey, D. E., *Continuous two stage, dual path anaerobic fermentation of butanol and other organic solvents using two different strains of bacteria*, US Patent 5753474, 1998.
[7] Yacoub, Y., Bara, R., Gautam, M., *The performance and emission characteristics of C1–C5 alcohol–gasoline blends with matched oxygen content in a single cylinder spark ignition engine*, Proc Inst Mech Eng A – Power Energy, Vol. 212, pp. 363–379, 1998.
[8] Gautam, M., Martin, D. W., *Emission characteristics of higher-alcohol/gasoline blends*, Proc Inst Mech Eng, Vol. 214A, pp. 165–182, 2000.
[9] Gautam, M., Martin, D. W., *Combustion characteristics of higher-alcohol/gasoline blends*, Proc Inst Mech Eng, Vol. 214A, pp.497–511, 2000.
[10] Dernotte, J., Mounaim-Rousselle, C., Halter, F., Seers, P., *Evaluation of Butanol–Gasoline Blends in a Port Fuel-injection, Spark-Ignition Engine*, Oil & Gas Science and Technology – Rev. IFP, Vol. 65 (2), pp. 345-351, 2010.
[11] Szwaja, S., Naber, J. D., *Combustion of n-butanol in a spark-ignition IC engine*, Fuel, Vol. 89, pp. 1573–1582, 2010.
[12] Alasfour, F. N., *NOx emission from a spark-ignition engine using 30% iso-butanol – gasoline blend: Part 1: Preheating inlet air*, Appl. Therm. Eng., Vol. 18 (5), pp. 245-256, 1998.
[13] Alasfour, F. N., *NOx emission from a spark-ignition engine using 30% iso-butanol – gasoline blend: Part 2: Ignition timing*, Appl. Therm. Eng., Vol. 18 (8), pp. 609-618, 1998.
[14] Broustail, G., Seers, P., Halter, F., Moréac, G., Mounaim-Rousselle, C., *Experimental determination of laminar burning velocity for butanol and ethanol iso-octane blends*, Fuel, Vol. 90, pp. 1–6, 2011.
[15] Yang, J., Wang, Y., Feng, R., *The Performance Analysis of an Engine Fueled with Butanol-Gasoline Blend*, Paper Number: 2011-01-1191, 2011.
[16] Heywood, J. B., *Internal Combustion Engine Fundamentals*, New York: McGraw-Hill, 1988.
[17] Brunt, M. F., Pond, C. R., Biundo J., *Gasoline Engine Knock Analysis using Cylinder Pressure Data*, SAE Paper No 980896, 1998.
[18] Mittal, V., Revier, B. M., Heywood, J. B., Phenomena that determine knock onset in spark-ignition engines, SAE Paper No. 2007-01-0007, 2007.
[19] Merola, S. S., Sementa, P., Tornatore, C., Vaglieco, B. M., Knocking diagnostics in the combustion chamber of boosted port fuel injection spark ignition optical engine, International Journal of Vehicle Design, Vol. 49 (1-3), pp.70–90, 2009.
[20] Merola, S. S., Sementa, P., Tornatore, C., *Experiments on knocking and abnormal combustion through optical diagnostics in a boosted spark ignition port fuel injection engine*, International Journal of Automotive Technology, Vol. 12, No. 1, pp. 93-101, 2011.
[21] Begg, S., Hindle, M., Cowell, T., Heikal, M., *Low intake valve lift in a port fuel-injected engine Energy*, the International Journal, Vol. 34 (12), pp. 2042-2050, 2008.
[22] Behnia, M., Milton, B. E., *Fundamentals of fuel film formation and motion in SI engine induction systems*, Energy Conv. and Manag., Vol. 42(15-17), pp. 1751-1768, 2001.
[23] Costanzo, V. S., Heywood, J. B., Mixture Preparation Mechanisms in a Port Fuel Injected *Engine*, SAE Technical Paper n. 2005-01-2080, 2005.
[24] Gold, M. R., Arcoumanis, C., Whitelaw, J. H., Gaade, J., Wallace, S., *Mixture Preparation Strategies in an Optical Four-Valve Port-Injected Gasoline Engine*, Int. J. of Engine Research, Vol. 1(1), pp. 41-56, 2000.

[25] Merola, S. S, Sementa, P, Tornatore, C., Vaglieco, B. M., *Effect of Fuel Injection Strategies on the Combustion Process in a PFI Boosted SI Engine*, Int. J. of Automotive Technology, Vol. 10(50), pp. 545−553, 2009.
[26] Merola, S. S, Sementa, P, Tornatore, C., Vaglieco, B. M., *Effect of Injection Phasing on Valves and Chamber Fuel Deposition Burning in a PFI Boosted Spark-Ignition Engine*, SAE International Journal of Fuels and Lubricants, Vol. 1 (1), pp. 192-200, 2009.
[27] Yang, J., Yang, X., Liu, J., Han, Z., Zhong, Z., *Dyno Test Investigations of Gasoline Engine Fueled with Butanol-Gasoline Blends*, SAE Paper no 2009-01-1891, 2009.
[28] Witze, P., Hall, M., Bennet, M., *Cycle-resolved Measurements of Flame Kernel Growth and Motion Correlated with Combustion Duration*, SAE paper n. 900023, 1990.
[29] Zhu, G. S., Reitz, R. D., Xin, J., Takabayashi T., *Modelling characteristics of gasoline wall films in the intake port of port fuel injection engines*, Int. J. Engine Research, Vol. 2 (4), pp. 231-248, 2001.
[30] Kim, H., Yoon, S., Lai, M. C., *Study of Correlation between Wetted Fuel Footprints on Combustion Chamber Walls and UBHC in Engine Start Processes*, Int. J. of Automotive Technology, Vol. 6 (5), pp. 437-444, 2005.